Palaeogeography, Palaeoclimatology, Palaeoecology 386 (2013) 86–95

Contents lists available at SciVerse ScienceDirect

Palaeogeography, Palaeoclimatology, Palaeoecology

journal homepage: www.elsevier.com/locate/palaeo

Validation of temperature–precipitation based aridity index: Paleoclimatic implications

Cheng Quan [a,*,1], Shuang Han [a], Torsten Utescher [b,c], Chunhua Zhang [d], Yu-Sheng (Christopher) Liu [e,**,1]

[a] Research Center of Paleontology and Stratigraphy, Jilin University, Changchun 130026, China
[b] Steinmann Institute, Bonn University, Bonn 53115, Germany
[c] Senckenberg Research Institute, Frankfurt 60325, Germany
[d] Department of Geography and Geology, Algoma University, Sault Ste. Marie, Ontario P6A 2G4, Canada
[e] Department of Biological Sciences, East Tennessee State University, Johnson City, TN 37614, USA

ARTICLE INFO

Article history:
Received 14 June 2012
Received in revised form 30 April 2013
Accepted 6 May 2013
Available online 16 May 2013

Keywords:
Paleoclimate
Aridity index
Mean annual temperature
Mean annual precipitation
Middle Miocene

ABSTRACT

Water availability in the ecosystem is one of the most crucial environmental factors that determines global terrestrial biome distribution. However, aridity/humidity conditions in the geologic past are difficult to quantify, mainly owing to the lack of a proper parameter. By using modern global climatic data, we here examine five selected previously proposed aridity indices (*AI*s), in which the climatic variables involved, including both precipitation and temperature, are simple and likely available in studies of paleoclimatology and paleoecology, although with different degrees of uncertainty. They were first evaluated along the modern climatic zones of eastern China, with the main metric of Thornthwaite humidity index (HI) and with the supplementary reference of soil moisture index (SMI) and near-ground atmospheric relative humidity (RH). Then *AI*s and the mean annual precipitation (MAP) were further statistically compared with HI, SMI, and RH, respectively, based on 1189 monitored data sets from meteorological stations over the world. The results show that the Köppen aridity index ($AI_{Köppen}$), expressed as mean annual precipitation divided by mean annual temperature plus a constant of 33, is the most accurate and precise index among all selected indices, supported by the highest correlation coefficient respectively to HI, SMI, and RH, three widely-employed major indicators sensitive to hydrological dynamics in climatology and meteorology. Specifically, $AI_{Köppen}$ does well mirror corresponding HI along four representative transects from North America, South America, Africa, and Australia, which cover the typical arid and humid climates and span the main terrestrial biome types. Moreover, our results also distinctly reveal that, as also shown by many studies on modern climate, precipitation alone is inadequate to measure the hydrological condition, because both temperature and evapotranspiration are two other critical factors that strongly influence water balance in the ecosystem, meanwhile evapotranspiration is mainly affected by temperature. Based on the validated $AI_{Köppen}$, we briefly discuss the aridity/humidity condition in China during the middle Miocene. The results demonstrate that moisture did decrease westward, but it is also clear that western China in the middle Miocene appears not to have been as dry as previously thought, indicated by the $AI_{Köppen}$ values representing a sub-humid to humid climate.

1. Introduction

In modern climatology and meteorology, most variables are unequivocally defined and can be quantitatively measured. Some of these variables, such as temperature and precipitation, might also be quantified from geologic proxies in paleoclimatic and paleoecological studies. However, there are other climatic variables that, although strongly impacting the ecosystem, have been ambiguously delineated and consequently difficult to be applied in paleoclimatology and paleoecology. Among all climatic factors, either aridity or humidity is one of the most critical contributors that controls the global terrestrial biome distribution, because no organism can live without water (Bugmann and Solomon, 2000; Woodward et al., 2004).

Although the term aridity is meteorologically related more or less to the drought condition of a given region in a particular period, there is still no generally accepted definition. Diverse definitions reflecting different disciplines have been proposed, such as in climatology, meteorology, hydrology, and agriculture (Wallén, 1967; Tuhkanen, 1980; Beran and Rodier, 1985; Wilhite and Glantz, 1985; Arora, 2002; Stadler, 2005; Shahid, 2010), in which the definition by Beran and Rodier (1985), referring the aridity of a given region to the deficiency of available water in the ecosystem, may be basically accepted. Quantitatively, it was Penck (1910) who first defined an arid region as the place where annual evaporation exceeds precipitation. This scheme was later

* Correspondence to: C. Quan, Research Center of Paleontology and Stratigraphy, Jilin University. 938, Xi-minzhu Str., Changchun, 130026, China. Tel.: +86 431 8860 5530; fax: +86 431 8850 2427.
** Correspondence to: Y.S. Liu, Department of Biological Sciences, 309 Brown Hall, East Tennessee State University, Box 70703, Johnson City, TN 37614-1710, USA. Tel.: +1 423 439 6920; fax: +1 423 439 5958.
E-mail addresses: quan@jlu.edu.cn (C. Quan), liuc@etsu.edu (Y.-S.(C.) Liu).
[1] The first and senior authors contributed equally to this study.

0031-0182/$ – see front matter © 2013 Elsevier B.V. All rights reserved.
http://dx.doi.org/10.1016/j.palaeo.2013.05.008

improved by including all possible evaporation and transpiration, i.e., the potential evapotranspiration (PET), and used as a humidity index (Thornthwaite, 1948). In modern climatology, the Thornthwaite humidity index (HI) is the most frequently adopted because it involves both inflows and outflows of water conditions, i.e., the effective precipitation. In the present study, we focus on the discussion of aridity index, rather than moisture or humidity index (see below for reasons). Once either of these indices is applied in paleoclimate studies, a refined quantification of terrestrial paleoclimate can be achieved.

Similar to the situation in modern climatology, the conceptual ambiguity of aridity has always been one of the main obstacles in paleoclimatic and paleoecological study which seriously hampers the estimation of paleo-aridity and hence the investigation of paleo-aridification. Because of the high immeasurability of evaporation/evapotranspiration from the geological record, and hence the unavailability of paleo-HI (e.g., Levin et al., 2006; Brachert et al., 2010), paleoclimatic studies have to deduce the deep time aridification by some water-sensitive indicators or by mean annual precipitation (MAP). Qualitative estimates of climate aridity have been inferred by either the occurrence of some possible characteristic sediments, e.g., red beds and evaporites (e.g., Sun and Wang, 2005; Abels et al., 2011), or the presence of xeric organisms, such as xerophytes (e.g., Hoorn et al., 2012). These qualitative indicators, in spite of their effectiveness to some extent, lack a uniform evaluation criterion to determine the true nature of arid condition and therefore prevent us from comprehensively understanding the aridification process throughout the geologic time.

Alternatively, a threshold value of MAP has been employed as the boundary between humid and arid environments in climatic classification (e.g., 500 mm; Penck, 1910; Lang, 1920; Walton, 1969; Sun and Wang, 2005). This scheme has been widely adopted in modern climatology because of the easy availability of data (e.g., Yan and Petit-Maire, 1994). However, precipitation alone is inadequate to measure the hydrological conditions of terrestrial climate (Thornthwaite, 1948; Walton, 1969; Warren, 2006; and see below). Two other critical factors that significantly affect water balance in ecosystems are temperature and evaporation (Thornthwaite, 1948; Walton, 1969; Botzan et al., 1998; Warren, 2006), with evaporation mainly determined by temperature and some other indirect factors, such as vegetation types (Thornthwaite, 1948; Warren, 2006). For example, it is intuitively clear that Juneau of Alaska should be drier than Miami of Florida due to the lower MAP (1387 mm vs. 1520 mm; Müller, 1996). However, the vegetation type of temperate rainforest in Juneau strongly suggests a much more humid climate than that of the tropical monsoon-dominated xeric-mesophytic hardwood landscape in Miami (Barbour and Billings, 2000; Kottek et al., 2006; Rubel and Kottek, 2010).

Likewise, if precipitation is used as the only indicator of deep time aridity/humidity, contrary conditions may be yielded from different proxies, such as lithological, isotopic, or paleontological data. For example, the widespread Miocene red beds and evaporites in northwestern China were considered to depict a mid-latitude drying period (Sun and Wang, 2005; Guo et al., 2008). But according to the land mammal data, it appears that this region was under a "humid" climate at that time, implied by both high mean molar teeth (hypsodonty) and enamel $\delta^{13}C$ data of herbivorous mammals (Fortelius and Zhang, 2006; Liu et al., 2009; Zhang et al., 2012). The relatively high precipitation qualitatively indicated by mammal fossils is further corroborated by a fossil plant-based quantitative paleoclimate reconstruction, showing that the Miocene MAPs of all studied areas in this region appear no less than 580 mm (Liu et al., 2011). This means that the high precipitation derived from the fossil evidence appears to conflict with the lithological records. However, it is still highly debated whether the so-called "environmentally sensitive" sediments (e.g., red beds and evaporites) necessarily indicate a lower precipitation and, therefore, an arid climate in the geologic past (Parrish, 1998; Yechieli and Wood, 2002; Ziegler et al., 2003).

Therefore, a critical question to ask is how we can better quantitatively estimate the arid/humid condition of a given region in the geologic past, and then make it possible to directly compare that with the modern climate using the same criterion. In this paper, we aim to evaluate several previously proposed aridity indices and validate an applicable one for paleoclimate study. By using modern global climatic data, we examine five precipitation-temperature defined aridity indices with the benchmark of PET-based HI, and finally validate the index of Köppen (1923) (see below for details). Based on the Köppen aridity index, a case study on the middle Miocene pattern of aridity and humidity in China is undertaken.

2. Materials and methods

2.1. Selection of aridity indices for evaluation

Aridity, unlike any other climatic parameters that can be directly monitored, is a result of interaction among several climatic factors, in which the precipitation and temperature jointly play a critical role (Wallén, 1967; Walton, 1969; Crago et al., 2005). In this paper, we refer the aridity of a given region as the deficiency of available water in the ecosystem (Beran and Rodier, 1985). The aridity index (*AI*), a dimensionless parameter, therefore represents a measure of water availability in the ecosystem of a region. In principle, the smaller the *AI* is, the drier the climate becomes, and vice versa.

To date, more than 50 empirical formulated indices have been proposed to represent this climate variable (summarized mainly in Tuhkanen, 1980; Stadler, 2005). Depending on the nature of the climate variables used, these indices can be largely divided into two groups, i.e., one involving only annual or monthly precipitation and temperature (PT), while the other further including potential evapotranspiration (PET) (for detail, refer to Tuhkanen, 1980; Stadler, 2005). Indices of either group have been widely used in modern climatic studies of various disciplines. However, PET-based indices are hardly applied in paleoclimatology due to the notorious unavailability of data for evaporation and/or evapotranspiration from geological records under current techniques (Levin et al., 2006; Brachert et al., 2010). Therefore, to find out a simple and practical *AI* for paleoclimate studies, we here have to exclusively evaluate the PT-based indices (Table 1), currently widely used in both Europe and America (e.g., Botzan et al., 1998; Arora, 2002; Tsakiris and Vangelis, 2004; Baltas, 2007; Shahid, 2010).

Five widely used PT-based indices are selected in the present study because in these indices the climatic parameters can be quantitatively reconstructed in paleoclimate studies (Table 1). Derived from Linsser's (1869) monthly humidity index (the ratio of monthly precipitation and temperature), Lang (1915, 1920) quantified *AI* as the ratio of MAP and mean annual temperature (MAT), based on the observation that the rise in temperature apparently increases the water deficit of soil and makes the air drier if not sufficiently recharged by precipitation and/or underground water (AI_{Lang}, Table 1). In this classification scheme, when MAT is above 0 °C, the climate of a given region is defined as arid with AI_{Lang} less than 40, as humid with AI_{Lang} between 40 and 160, and as perhumid with AI_{Lang} larger than 160 (Lang, 1920). When MAT is below 0 °C, the climate is subdivided into the nival (Nivales), cold weather (Kälteverwitterung), and frost (Frosterden) by the MAP with limiting boundaries of 2000 mm and 5000 mm, respectively (Lang, 1920).

de Martonne (1926) slightly modified Lang's (1915, 1920) aridity formula of MAP/MAT ratio by adding a constant of 10 to MAT in the denominator (AI_{dM}, Table 1). Later, de Martonne (1942) developed his second aridity index by including both annual and coldest month temperatures, and corresponding precipitation level ($AI_{dM\text{-}2}$, Table 1).

Emberger (1930) devised another index to categorize aridity (pluviothermic index), which includes the mean annual range of temperature ($AI_{Emberger}$, Table 1), and shows a direct relation to evaporation in some climatic provinces.

Table 1
Selected aridity indices (*AI*).

Index	Classification	Remarks	Reference
(1) $AI_{\mathrm{Lang}} = \frac{MAP}{MAT}$	AI_{Lang} < 40: arid; 40–160: humid; >160, perhumid	Practicable only when the mean annual temperature (MAT, °C) is above 0 °C; MAP—the mean annual precipitation (mm)	Lang (1920)
(2) $AI_{\mathrm{KÖppen}} = \frac{MAP}{MAT+33}$	—	MAP in mm; MAT in °C	Köppen (1923)
(3) $AI_{\mathrm{dM}} = \frac{MAP}{MAT+10}$	AI_{dM} < 5: arid; 5–10: semi-arid; 10–20: semi-humid; 20–30: humid; >30: perhumid	MAP in mm; MAT in °C	de Martonne (1926)
(4) $AI_{\mathrm{Emberger}} = \frac{100\times MAP}{WMT^2-CMT^2}$	—	MAP in mm; WMT—the warmest month absolute temperature (°K); CMT—the coldest month temperature (°K)	Emberger (1930)
(5) $AI_{\mathrm{dM-2}} = \frac{MAP}{MAT+10} + \frac{12\times DMP/(DMT+10)}{2}$	—	DMP—the lowest month precipitation (mm); DMT—the temperature of the month with lowest precipitation (mm); MAP in mm; MAT in °C	de Martonne (1942)

Köppen (1923) proposed his aridity index which is also based on the principle of AI_{Lang}. This index, long overlooked probably because of its similarity to AI_{dM}, is also included in the present study ($AI_{\mathrm{Köppen}}$, Table 1).

It should be mentioned that Köppen (1931) also devised another scheme to classify the world climates, in which the ardity index takes account of seasonal precipitation because the rainfall in warm months is less effective than the same amount of precipitation occurring in the cold months. However, this index is excluded in the present study because it requires a pre-determination of seasonality for a given area. Although the annual distribution of either thermal or hydrological alternation in a certain region is easy to determine in modern climates, information of seasonal dynamics of temperature and precipitation is difficult to extract from geological records in many cases, particularly those based on either isotopes or mammal fossils (e.g., Fortelius and Zhang, 2006; Zhang et al., 2012).

2.2. Data sources and processing

The long-term modern global climate data, such as monitored long-term means of temperature, precipitation, and RH, were mainly taken from Müller (1996), with supplementary data from China that are available on the website of the China Meteorological Data Sharing Service System (open access to registered user at http://cdc.cma.gov.cn/; years of 1971–2000; Appendix A). A total of 1189 datasets from individual meteorological stations were compiled, representing all continents except Antarctica (Appendiex B). Corresponding HI and SMI data of each climate station were extracted from gridded global datasets. The global HI data were from the Consortium for Spatial Information, Consultative Group on International Agricultural Research (CGIAR-CSI; http://www.cgiar-csi.org/; long-term mean years 1950–2000), while the corresponding temperature and precipitation data used to calculate the global aridity distribution were from WorldClim (http://www.worldclim.org/). The global SMI database is available on the website of the Earth System Research Laboratory, National Oceanic and Atmospheric Administration (ESRL of NOAA; http://esrl.noaa.gov/; long-term mean of years 1948–2000).

World maps were produced using ArcGIS 10 (ESRI, USA) with the spatial resolution of 0.1° in WGS-1984 geographic coordinate system. The statistical analyses were produced by IBM SPSS (IBM SPSS Inc., USA).

2.3. Methods

To evaluate these indices, we used the Thornthwaite humidity index (HI) as the main benchmark. The HI is the most widely accepted criterion for describing the aridity/humidity condition of modern climates, because it involves both inflows (e.g., precipitation and subsurface influx) and outflows (e.g., evapotranspiration, runoff, and drainage) (Thornthwaite, 1948). This PET-based index is defined by the ratio of annual precipitation and potential evapotranspiration as MAP/PET (Thornthwaite, 1948). The evaluation of these *AI*s is further undertaken by comparing them with the PET-based soil moisture index (SMI) and monitored near-ground atmospheric relative humidity (RH). The reason for further evaluation is because the PET-based SMI largely couples with the climatic variability (Murphy and Timbal, 2008), while the RH is highly sensitive to climate change and water dynamics (Schneider et al., 2010).

We first visually test each *AI* across eastern China to find out its general trend in comparison to HI, SMI, and RH, respecitvely (data available in Appendix A). Eastern China has been chosen because it clearly represents one of the most complete spectra of climatic zones in the North Hemisphere (Walton, 1969; Walter, 1973), where the climate is considered to be humid in the south and becomes arid in the north (Fang and Yoda, 1989).

To statistically compare each *AI* with HI, SMI, and RH respectively, we further compiled monitered precipitation-temperature data sets, and conducted correlation analyses to find out the most effective *AI*.

Global aridity distribution was then calculated by the validated *AI* and compared with the global HI, the most widely adopted PET-based index in describing modern aridity/humidity. Moreover, we selected four representative transects around the world to further discuss the accuracy of validated *AI* with the benchmark of HI. These four transects were selected because they cover the typical arid and humid climates and span the main terrestrial biome types in the Köppen–Geiger climate classification (Kottek et al., 2006; Peel et al., 2007; Rubel and Kottek, 2010).

3. Results

3.1. AIs along zonal climates

In the climatic zones of eastern China, aridity/humidity indicators of HI, SMI, and RH show a general trend of northward drying (Fig. 1A–C; Appendix A). However, the calculated *AI*s show individual features (Fig. 1D–H). As illustrated in Fig. 1, it is evident that the primary trends of AI_{Lang} and AI_{Emberger} across eastern China are not consistent with either HI and SMI, or RH (compare Fig. 1D and F with A–C). AI_{dM} has a comparable trend especially with those of HI and RH, but it appears to be more scattered than either (Fig. 1A, C and E). $AI_{\mathrm{dM-2}}$ also well represents the zonal climatic pattern of eastern China (Fig. 1G). However, some parameters used in $AI_{\mathrm{dM-2}}$ are not always available in paleoclimatic studies (see below). Of all selected *AI*s, $AI_{\mathrm{Köppen}}$ values show the most compatible pattern among the selected PT-based formulae to both HI and RH along the latitudinal climate zonation (Fig. 1H).

For statistical comparison, we further conducted a paired correlation analysis between the selected *AI*s, MAP, HI, SMI, and RH. A total of 1189 sets of climatic data were assembled from meteorological stations in

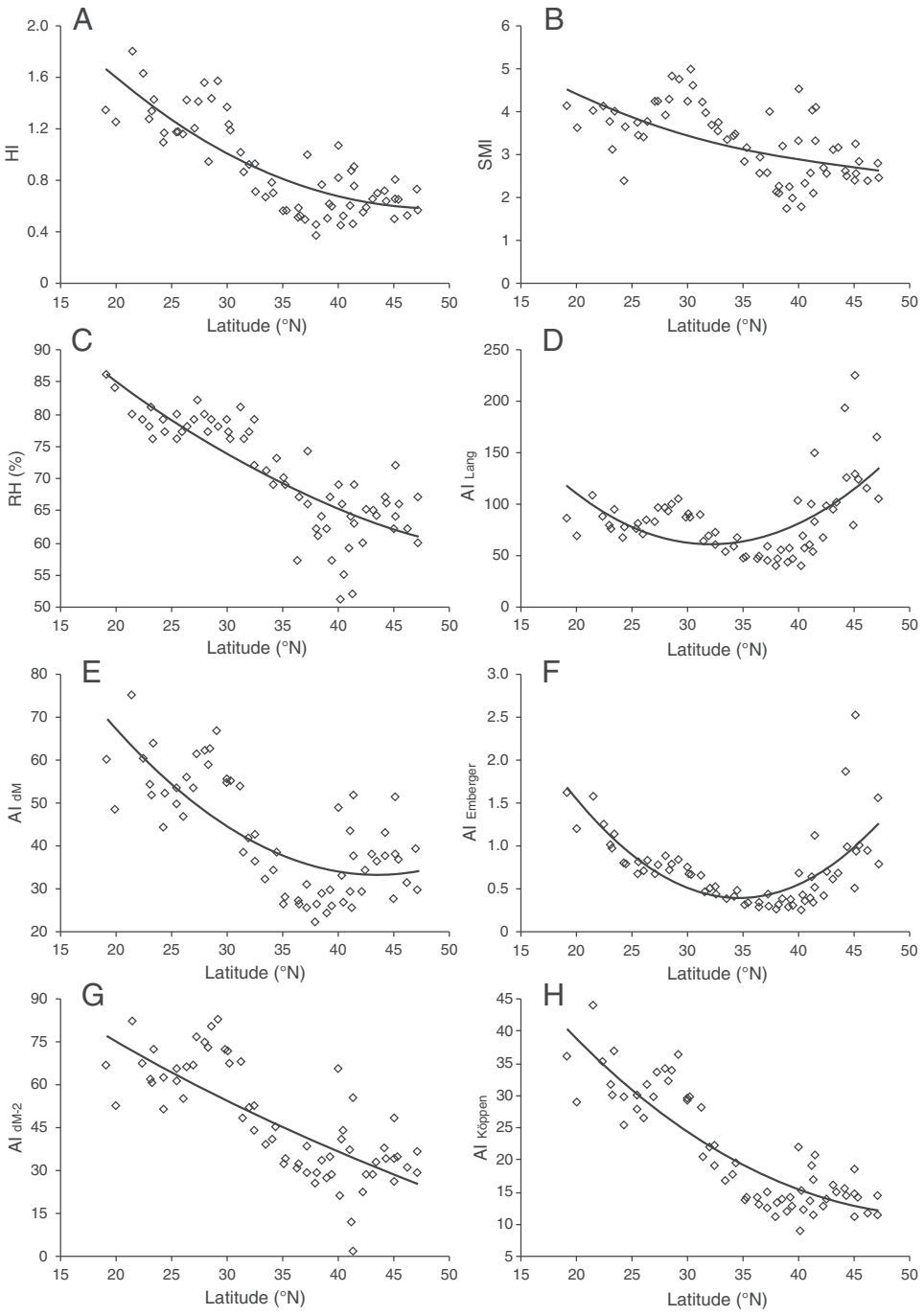

Fig. 1. Latitudinal comparison between the Thornthwaite humidity index (HI), soil moisture index (SMI), and atmospheric relative humidity (RH) and five selected aridity indices along the zonal climate of eastern China. A–C, latitudinal distribution of HI, SMI, and RH, respectively. D–H, distribution of each *AI* against latidude. The data of HI, SMI, RH and the corresponding temperature and precipitation of each site (open diamond) are listed in Appendix A. Solid line of each chart shows the general trend of the data.

Africa, Asia, Australia, North America, and South America (Appendix B). As clearly shown in Table 2, among all the selected *AI*s and MAP, $AI_{\text{Köppen}}$ yields the highest Pearson correlation coefficient separately for HI, SMI, and RH (0.8168, 0.6700, and 0.5582, respectively; $p < 0.01$) and mostly low standard deviation and error mean. These results strongly suggest that 1) $AI_{\text{Köppen}}$ is more effective in describing climatic aridity/humidity conditions than the solo parameter of MAP, and 2) $AI_{\text{Köppen}}$ is the most reliable aridity index based on precipitation and temperature, in which both parameters in the formula, MAT and MAP, are most likely to be available in paleoclimate studies.

3.2. Testing $AI_{\text{Köppen}}$ in extant terrestrial biomes

To test $AI_{\text{Köppen}}$ on a global scale, we produced the world map of $AI_{\text{Köppen}}$ distribution (Fig. 2A), and compared it to the PET-based HI distribution (Fig. 2B). We further selected 4 transects from North America, South America, Africa, and Australia respectively to evaluate the reliability of $AI_{\text{Köppen}}$. These transects cover a typical humid to arid climate ranging from rainforest to desert (transects T1–T4 in Fig. 2B).

As demonstrated in Fig. 2, the global configuration of $AI_{\text{Köppen}}$ matches the overall pattern of the HI. The global distribution of $AI_{\text{Köppen}}$ shows that the most humid region is in tropical or temperate

Table 2
Paired correlation among the selected aridity indices, mean annual precipittion (MAP), Thornthwaite humidity index (HI), soil moisture index (SMI), and atmospheric relative humidity (RH). Monitored long-term climatic data are compiled from Müller (1996) and China Meteorological Data Sharing Service System (open access to registered user; http://cdc.cma.gov.cn/). Data are from 1189 meteorological stations and available in Appendix B.

Parameter		AI_{Lang}	AI_{dM}	$AI_{Emberger}$	AI_{dM-2}	$AI_{Köppen}$	MAP
HI	Pearson correlation	0.0244*	0.5332**	0.0968**	0.3193**	0.8168**	0.6844**
	Sig. (2-tailed)	0.4014	0.0000	0.0008	0.0000	0.0000	0.0000
	Std. deviation	747.8100	46.2563	7.3159	96.9228	12.0799	718.1753
	Std. error mean	21.6870	1.3415	0.2122	2.8108	0.3503	20.8276
SMI	Pearson correlation	0.0392*	0.4051**	0.1413**	0.2538**	0.6700**	0.5853**
	Sig. (2-tailed)	0.1770	0.0000	0.0000	0.0000	0.0000	0.0000
	Std. deviation	747.7584	45.9166	7.3140	96.6977	11.5027	717.5918
	Std. error mean	21.6855	1.3316	0.2121	2.8043	0.3336	20.8107
RH	Pearson correlation	0.0512*	0.3033**	0.1260**	0.1845**	0.5582**	0.4840**
	Sig. (2-tailed)	0.0778	0.0000	0.0000	0.0000	0.0000	0.0000
	Std. deviation	747.3134	44.4711	13.1326	95.6587	11.5193	712.9717
	Std. error mean	21.6726	1.2897	0.3809	2.7742	0.3341	20.6767

*Correlation is significant at the 0.05 level ($p < 0.05$).
**Correlation is significant at the 0.01 level ($p < 0.01$); sample size = 1189.

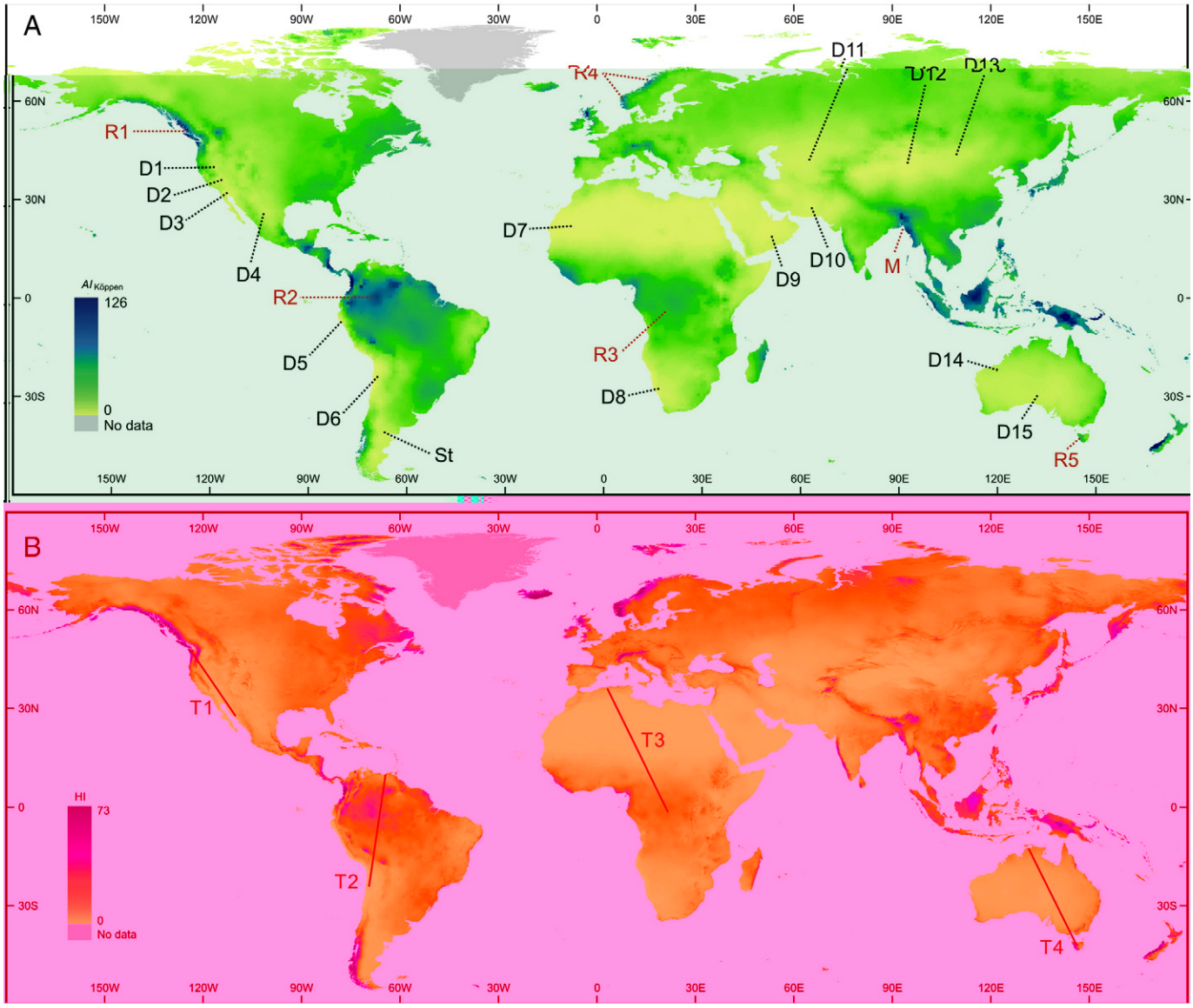

Fig. 2. Global comparison between $AI_{Köppen}$ and Thornthwaite humidity index (HI) and soil moisture index (SMI). A, Global arid-humid distribution indicated by $AI_{Köppen}$, showing the driest region in deserts and the most humid region corresponding to ecosystems of rainforests and mangroves. Main deserts: D1—Great Basin; D2—Mojave; D3—Sonoran; D4—Chihuahuan; D5—Sechura; D6—Atacama; D7—Sahara; D8—Kalahari and Namib; D9—Arabian; D10—Lut and Thar; D11—Karakum; D12—Taklimakan; D13—Gobi; D14—Great Sandy, Gibson, and Tanami; D15—Great Victoria, Simpson, and Tirari-Sturt stony. Rainforests and mangrove: R1—North Pacific temperate rainforest; R2—Amazon tropical rainforest; R3—Congo River Basin tropical rainforest; R4—Scandinavian coastal temperate rainforest; R5—Tasmanian temperate rainforest; M—Bangladesh mangrove. B, global HI. T1–T4 showing the 4 selected transects that cover the main biome types around the world.

rainforests, while the arid regions overlap the deserts. In North America, the most humid climate indicated by $AI_{Köppen}$ is in the Pacific Northwest Temperate Rainforest along the coast range of the southeastern Gulf of Alaska and northwestern British Columbia, Canada (R1 in Fig. 2A), whereas the outstanding arid regions are in the Great Basin, Mojave, and Sonoran deserts, including central-southeastern California, southern Nevada, southwestern Utah, and northwestern Arizona, and northern-northwestern Mexico (D1–D4 in Fig. 2A). Longitudinally, the climate of the eastern middle latitudes of North America is generally wetter than that of the west (Fig. 2A). This suggests that $AI_{Köppen}$ can be considered a close analogue of HI. This relationship is further confirmed by 4 selected large-scaled transects across typical arid-humid biome transitions (Figs. 2B and 3; Table 3). In transect T1 (North America), $AI_{Köppen}$ declines southward, from 46.3 in the Pacific Northwest Temperate Rainforest to 3.1 in the Sonoran Desert, which is consistent with the HI results (Fig. 3A). Along transect T2 (South America), the most humid area indicated by $AI_{Köppen}$ is in the middle-north part with values more than 24, coupled with the biome of the Amazon Rainforest. The driest climate is found in the Atacama Desert in the south with $AI_{Köppen}$ of 0.02, while moderate humid conditions correspond to the tropical savanna climate in the north with $AI_{Köppen}$ of 15.5. The overall $AI_{Köppen}$ trend of transect T2 is also corroborated by the HI (Fig. 3B).

Transect T3 represents well the latitudinal climatic distribution of Africa, from the moderately humid Mediterranean climate of the coast in the north with $AI_{Köppen}$ of 4.6–17.9, very arid condition in the Sahara Desert in the middle-north with $AI_{Köppen}$ less than 0.8, hot semi-arid to sub-humid conditions of the steppe and tropical deciduous forest-woodland savanna biomes in the middle-south with $AI_{Köppen}$ of 16.9–28.3, to the tropical rainforest of the Congo River Basin in the south. The distribution pattern of humidity along T3 is strongly supported by HI (Fig. 3C).

$AI_{Köppen}$ distribution of Australian climate (T4 in Fig. 2B; Fig. 3D) matches well with that of the Köppen climatic classification (refer to Kottek et al., 2006; Peel et al., 2007), showing the effect of continentality, largely with humid conditions along the coast and an arid climate in the central regions. As seen in section T4 (Fig. 3D), both $AI_{Köppen}$ and HI indicate the relatively humid climates of tropical monsoonal savanna in the north and temperate rainforest in the south, but arid conditions in the central deserts.

In summary, our results show that among MAP and the various *AI*s we analyzed, $AI_{Köppen}$ is the most effective index for reconstructing climatic aridity/humidity conditions. There is a very strong correlation between $AI_{Köppen}$ and HI ($r = 0.8168$, $p < 0.01$; globally). Additionally, in comparison with other indices examined, $AI_{Köppen}$ has the strongest correlation with both SMI and RH (Table 2). Furthermore, $AI_{Köppen}$ requires the least number of climatic parameters, i.e., MAT and MAP, which can likely be estimated in terrestrial paleoclimate studies (e.g., Wing and Greenwood, 1993; Wilf, 1997; Greenwood et al., 2010; Utescher et al., 2011). Therefore, $AI_{Köppen}$ can be used in paleo-aridity reconstruction assuming that the deep time MAT and MAP had similar impacts on the aridity of a given area, with a high value of $AI_{Köppen}$ in a humid climate and low value in an arid region. In the modern HI scheme, the global climate is generally classified into 5 aridity/humidity conditions by particular threshold values (Thornthwaite, 1948) (Table 4). According to the corresponding mean value of each threshold, the $AI_{Köppen}$ category based on the present global dataset is given in Table 4.

4. Discussion

From the aspect of biome, living organisms, especially terrestrial plants, are highly subjected to the influence of climate. Consequently, terrestrial biomes show a strong correlation between latitudinal zonation and climate distribution (Walter, 1973; Woodward et al., 2004). This offers qualitative evidence to aridity/humidity index evaluation, because precipitation and temperature, two inputs for *AI*s, play a key role in the terrestrial biome distribution, as shown in the present study. The $AI_{Köppen}$ pattern of North America is strongly supported by the regional distribution of vegetation, from the tidal wetland forests in the southeast, temperate deciduous forests in the east, grassland in the Great Plains, to warm deserts in the West (Barbour and Billings, 2000; Light et al., 2002). In South America, the boundary of the most humid region delimited by $AI_{Köppen}$ largely corresponds to that of the tropical rainforest (see Fine et al., 2008), whereas the most arid region

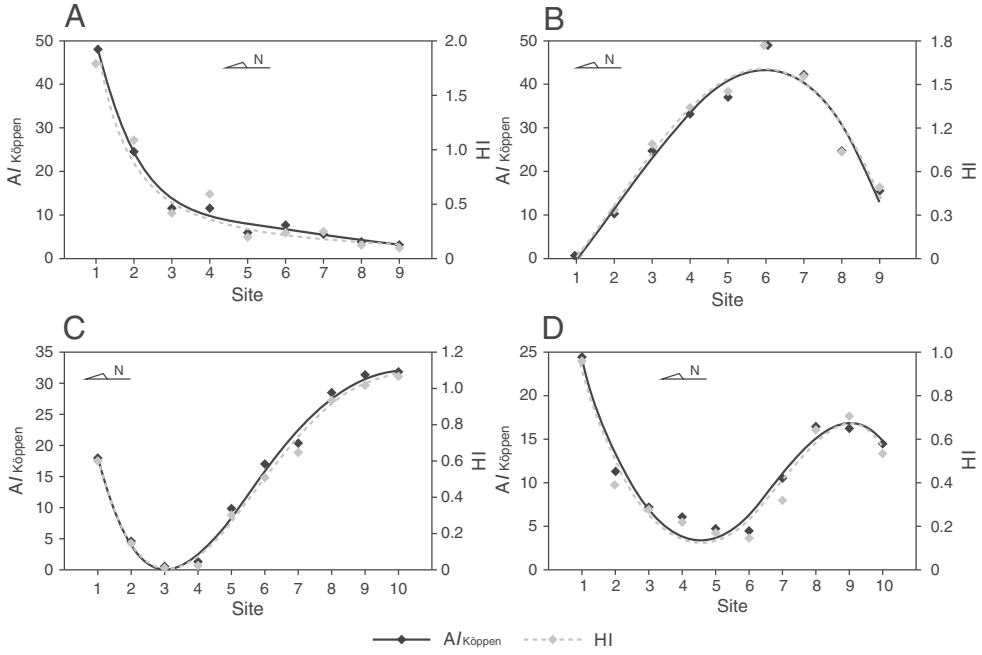

Fig. 3. Transect comparison between $AI_{Köppen}$ and Thornthwaite humidity index (HI) across the main biome types. Each chart illustrates the value of $AI_{Köppen}$ (black solid diamonds) and its corresponding HI of the sites (gray open diamonds) along the transect as shown in Fig. 2; data as in Table 4. Black solid line and gray dash show the overall trend of particular transect respectively by $AI_{Köppen}$ and the corresponding HI. A, transect T1, North America; B, transact T2, South America; C, transect T4, Africa; D, transect T4, Australia.

Table 3
Climatic data, $AI_{Köppen}$, and Thornthwaite humidity index (HI) along 4 selected transects (T1–T4).

No.	Location	Lat.	Long.	Climate type	MAT (°C)	MAP (mm)	$AI_{Köppen}$	HI
T1 (North America)								
1	Tatoosh Island, Washington	48°23′	−124°44′	Csb	9.6	1973	46.3	1.79
2	Portland, Oregon	45°32′	−122°40′	Csb	12.6	1075	23.6	1.08
3	Medford, Oregon	42°22′	−122°52′	Csa	11.9	502	11.2	0.42
4	San Francisco, California	37°47′	−122°25′	Csb	13.8	529	11.3	0.59
5	Fresno, California	36°46′	−119°42′	BSk	16.8	285	5.7	0.20
6	Los Angeles, California	34°3′	−118°14′	Csa	18	373	7.3	0.25
7	San Diego, California	32°44′	−117°10′	BSk	17.2	264	5.3	0.25
8	Guaymas, Mexico	27°55′	−110°53′	BWh	25	222	3.8	0.12
9	La Paz, Mexico	24°10′	−110°18′	BWh	24.2	179	3.1	0.11
T2 (South America)								
1	Arica, Chile	−18°28′	−70°22′	BWh	18.8	1	0.02	0.01
2	La Paz, Bolivia	−16°30′	−68°8′	Cwb	10.4	448	10.3	0.47
3	Apolo, Bolivia	−14°43′	−68°30′	Aw	20.3	1324	24.8	0.89
4	Puerto Maldonado, Peru	−12°38′	−69°12′	Aw	25.3	1927	33.1	1.28
5	Sena Madureira, Brazil	−9°8′	−68°40′	Am	24.7	2138	37.1	1.42
6	Uaupes, Brazil	−0°8′	−67°5′	Af	25.4	2869	49.1	1.78
7	Puerto Ayacuacho, Venezuela	5°41′	−67°38′	Aw	27.2	2549	42.3	1.51
8	San Fernando de Apure, Venezuela	7°53′	−67°26′	Aw	27.1	1491	24.8	0.88
9	Caracas, Venezuela	10°30′	−66°56′	Aw	21	835	15.5	0.60
T3 (Africa)								
1	Tanger, Morocco	35°43′	5°54′	Csa	16.9	895	17.9	0.60
2	Marrakech, Morocco	31°36′	8°1′	BSh	19.9	241	4.6	0.15
3	Adrar, Algeria	27°52′	0°20′	BWh	24.5	18	0.3	0.01
4	Tamanrasset, Algeria	22°42′	5°31′	BWh	21.2	44	0.8	0.02
5	Maiduguri, Nigeria	11°51′	13°5′	BSh	27.6	590	9.7	0.30
6	Garoua, Cameroon	9°20′	13°23′	Aw	27.2	1015	16.9	0.51
7	Moundou, Chad	8°37′	16°4′	Aw	27.6	1228	20.3	0.64
8	Batouri, Cameron	4°22′	18°34′	Aw	23.7	1605	28.3	0.90
9	Bongabo, Zaire	3°6′	20°32′	Af	24.9	1810	31.3	1.02
10	Yangambi, Zaire	0°49′	24°29′	Af	24.6	1828	31.8	1.07
T4 (Australia)								
1	Darwin	−12°28′	130°51′	Aw	28	1490	24.4	0.96
2	Wyndham	−15°27′	128°7′	BSh	29.1	703	11.3	0.39
3	Halls Creek	−18°13′	127°46′	BSh	25.6	423	7.2	0.28
4	Tennant Creek	−19°34′	134°13′	BWh	25.2	352	6.1	0.21
5	Alice Springs	−23°42′	133°53′	BWh	20.6	252	4.7	0.17
6	Port Augusta	−32°29′	137°45′	BWh	19	236	4.5	0.14
7	Adelaide	−34°56′	138°35′	Csa	16.7	523	10.5	0.32
8	Mount Gambier	−37°50′	140°46′	Csb	13.9	774	16.5	0.65
9	Launceston	−41°27′	147°10′	Cfb	12.7	742	16.2	0.71
10	Hobart	−42°53′	147°20′	Cfb	12.2	654	14.5	0.53

is located along the eastern coast of the Pacific and the southwestern part of South America (Fig. 2A).

The most humid climates on the Eurasian continent depicted by $AI_{Köppen}$ prevail the Scandinavian coastal temperate rainforest and the Bangladesh mangrove ecoregions (Fig. 2A), whereas the extreme arid regions incorporate almost all deserts from the Arab Peninsula (the Arabian Desert), Middle East (Lut and Thar deserts), West Asia (Karakum Desert), and Central Asia (Taklimakan Desert) to East Asia (Gobi Desert) (Fig. 2A).

The African climate represents the typical latitudinal distribution of aridity/humidity (Gasse, 2000; this study, Fig. 2), ecologically marked by the tropical rainforest in the middle, and the Sahara and Kalahari deserts in the north and southwest, respectively (Fig. 2A).

Table 4
Categories of climate condition based on Thornthwaite humidity index (HI) and $AI_{Köppen}$.

	Hyper-arid	Arid	Semi-arid	Sub-humid	Humid
HI	<0.03	0.03–0.2	0.2–0.5	0.5–0.65	>0.65
$AI_{Köppen}$	<0.9	0.9–5.7	5.7–13.6	13.6–15.6	>15.6

Although the climate of Australia varies from the tropical monsoon in the North to cool temperate in the South (Tasmania) (Jeffrey et al., 2001), its general distribution pattern relates to the impact of continentality, which largely results in an arid interior desert insulated from oceanic influences, and a humid coast effected by wet onshore air masses that originate over oceans (Figs. 2 and 3D).

For evaluated *AI*s, AI_{Lang} is the first index using climatic parameters of precipitation and temperature (PT) to quantitatively measure aridity. Many PT-based indices have been derived from AI_{Lang}. However, AI_{Lang} is not efficient in indicating aridity in eastern China (Fig. 1). Moreover, it appears that AI_{Lang} works only when MAT is above 0 °C. It fails to describe the aridity conditions in the subdivision of freezing climate with negative MAT. The non-absorbable snow and ice in the winter become available to biomes in the summer (de Martonne, 1926).

To avoid the disadvantage of negative index values automatically obtained with MAT below 0 °C when classifying the European climate, in particular around the Mediterranean regions, de Martonne (1926) slightly modified Lang's (1915, 1920) aridity formula of MAP/MAT ratio by adding a constant of 10 to MAT in the denominator, assuming that the lowest European MAT is about −10 °C. AI_{dM} has widely been used in modern studies to describe the drought condition or

aridification processes of a given region, especially in large scale investigations because of its minimal data requirement (Botzan, 1974; Roberts, 1993; Arora, 2002; Tsakiris and Vangelis, 2004; Baltas, 2007; Shahid, 2010). For example, Botzan (1974) developed a new concept in agricultural drought based on the hydroclimatic characteristics defined by AI_{dM}.

However, in spite of the virtue of AI_{dM}, its disadvantage is apparently at the extremity of the equation at MAT of −10 °C, where the index is undefined. Moreover, the value of AI_{dM} would become exceptionally large when the MAT approaches −10 °C (e.g., −9.8 °C), but the freezing climate is not always as humid as indicated by the large value of AI_{dM} because the water in a frozen region is mainly in a solid condition, basically unavailable to organisms in the ecosystem/biome (e.g., Chaves et al., 2003). This might be the reason that AI_{dM}, a widely used PT-based index, yields a relatively low correlation coefficient with regard to that of $AI_{Köppen}$, and even lower than obtained for MAP alone, one of the parameters in the formula (Table 2).

Moreno et al. (1990) found that $AI_{Emberger}$ is a good indicator for biogeographical classification in Europe, because the bioclimatic belts and the main vegetation types in the Iberian Peninsula are largely discriminated by $AI_{Emberger}$. This result is also supported by independent studies, although some discrepancies exist in demonstrating a relationship between the thermal-hydrological condition and vegetation (Retuerto and Carballeira, 1992). Methodologically, $AI_{Emberger}$ uses Kelvin degree (absolute temperature, in K) to avoid negative values (Table 1). However, this does not always work, especially in upper mid-latitude regions (Appendix B). In addition, as shown in the present study, $AI_{Emberger}$ is not always as effective as expected. Especially along climatic zones, it yields almost a reverse trend in comparison to those of HI, SMI, and RH (Fig. 1). This inconsistency appears to be due to the northward increased mean annual range of temperature, especially in the middle and high latitudes (Appendices A and B).

$AI_{dM\text{-}2}$ is an index that had been suggested to work well, especially for large-scale studies, such as the 1:50,000,000 world map of aridity distribution (de Martonne, 1942), which matches well the Köppen–Geiger climate map (Kottek et al., 2006; Peel et al., 2007). This index also well represents the zonal climatic pattern of eastern China (Fig. 1G). However, in paleoclimate studies, although two of the parameters in the formula, i.e., the precipitation and temperature of the month with lowest rainfall (DMP and DMT, respectively; Table 1), are sometimes replaced by the winter temperature and winter precipitation, respectively (e.g., Akkiraz et al., 2011), they are hardly available for use in current quantitative techniques of paleoclimate reconstructions, such as the leaf margin analysis and leaf area analysis (Wing and Greenwood, 1993; Wilf, 1997; Greenwood et al., 2010; Su et al., 2010), coexistence approach (Mosbrugger and Utescher, 1997; Liu et al., 2011; Utescher et al., 2011; Quan et al., 2012b), climate leaf analysis multivariate program (Wolfe, 1993; Spicer et al., 2009), and isotope-based methods (Zhang et al., 2012).

The relationship between the vegetation type and aridity/humidity conditions has long been recognized, as shown by the closely fitting boundaries between climatological and phytogeographical maps (Tuhkanen, 1980). In his innovative study, Köppen (1900) qualitatively defined arid regions by the presence of xerophilous plants, such as *Agave*, *Nitraria*, *Welwitschia*, and *Opuntia*, and particularly emphasized the impacts of temperature-moisture fluctuations on vegetation formations in desert and steppe regions. Later, Köppen (1923) proposed his aridity index ($AI_{Köppen}$), which is also based on the principle of AI_{Lang}. However, this index has long been overlooked probably because of its similarity to AI_{dM}. In $AI_{Köppen}$, the MAT in the denominator is added by a constant of 33 by which the boundary between deserts and steppes is well defined by $AI_{Köppen}$ (Köppen, 1923). Additionally, the constant 33 in the denominator adequately offsets the low MAT and avoids negative index values, which makes it possible to compare aridity condition at a global scale by using $AI_{Köppen}$ (Figs. 1–3; Table 2).

5. $AI_{Köppen}$ for paleoclimate: a case study on the middle Miocene of China

As mentioned above, in northwestern China widespread red beds and evaporites developed from the Oligocene to the Quaternary appear to imply substantial aridity events in the Asian interior during this period (Liu et al., 2009; Abels et al., 2011). However, the paleoclimate reconstructions based on either mammal or plant fossils demonstrate that the northern Tibetan Plateau had received relatively high MAP during the Miocene. Fortelius and Zhang (2006) proposed that the high MAP resulted from oases in the desert. Ecologically, however, the primary productivity of oases might not be able to support such diverse mammal communities in the region. We here test the middle Miocene aridity variation from eastern to western China by $AI_{Köppen}$ to find out its overall hydrological pattern. We hypothesize that the west, lithologically characterized by the red beds and evaporites (Liu et al., 2009), was more arid than the east that was climatologically dominated by the East Asian monsoon (Sun and Wang, 2005).

Consistent with the hypothesis, results from five selected middle Miocene localities in China (Fig. 2B) show that the middle Miocene aridity increased westward (Table 5 and Fig. 4). The relatively low $AI_{Köppen}$ in the west demonstrates that western China appears drier than the east. It also suggests that the climate from eastern to western China experienced an asymmetric process of aridification from the middle Miocene to the present (Fig. 4). In the east the aridity intensified slightly from the middle Miocene ($AI_{Köppen}$ = 23.5) to that at present with ($AI_{Köppen}$ = 21.6; Site 5 in Table 5 and Figs. 2B and 4), whereas in central China the aridification enhanced moderately, with $AI_{Köppen}$ declining from 24.6 to 14.0 (Table 4 and Fig. 4). However, significant aridification is observed in the west, with $AI_{Köppen}$ decreasing at least 10.2 (from 19.5 to 9.3; Site 3 in Table 5), similar to the difference between Seattle of Washington and Cheyenne of Wyoming, USA, strictly in terms of aridity/humidity (with $AI_{Köppen}$ of 19.3 and 9.4, respectively; Appendix B).

However, despite the westward aridification during the middle Miocene, it is also clear that western China was not as dry as previously thought. All $AI_{Köppen}$ values of the three western sites are larger than 13.6, the boundary between semi-arid and sub-humid climates, indicating the sub-humid to humid climates according to the $AI_{Köppen}$ category (Sites 1–3; Tables 4 and 5). These $AI_{Köppen}$ results are highly congruent with the data based on either mammal or plant fossils (Fortelius and Zhang, 2006; Liu et al., 2011; Zhang et al., 2012). Therefore, although western China was more arid than the east, it appears that the sub-humid to humid climate there provided sufficient water during the middle Miocene to support those mammals and plants recorded as fossils.

The results of the case study suggest that sedimentology alone may not always be able to indicate the aridity condition of deep time. Besides, in comparison to $AI_{Köppen}$, reconstructed MAP and MAP-related isotopic

Table 5
Paleoclimate data and $AI_{Köppen}$ values of the five mid Miocene fossil localities of Chin and corresponding modern data. Paleoclimate data are from Liu et al. (2011); the mean annual temperature (MAT) in °C and the mean annual precipitation (MAP) in mm.

Site no.	Location	Coordinates	Mid Miocene			Modern		
			MAT	MAP	$AI_{Köppen}$	MAT	MAP	$AI_{Köppen}$
1	Taxihe, Xinjiang	44°30′N, 85°30′E	15.0	698	14.5	7.6	133	3.3
2	Dunhuang, Gansu	40°42′N, 94°43′E	16.8	979	19.7	10.2	40	0.9
3	Chetougou, Qinghai	36°18′N, 101°44′E	15.6	947	19.5	7.8	380	9.3
4	Zhoukou Basin, Henan	33°31′N, 114°38′E	14.3	1164	24.6	14.5	663	14.0
5	Tianchang, Jiangsu	32°44′N, 118°41′E	15.9	1151	23.5	15.3	1041	21.6

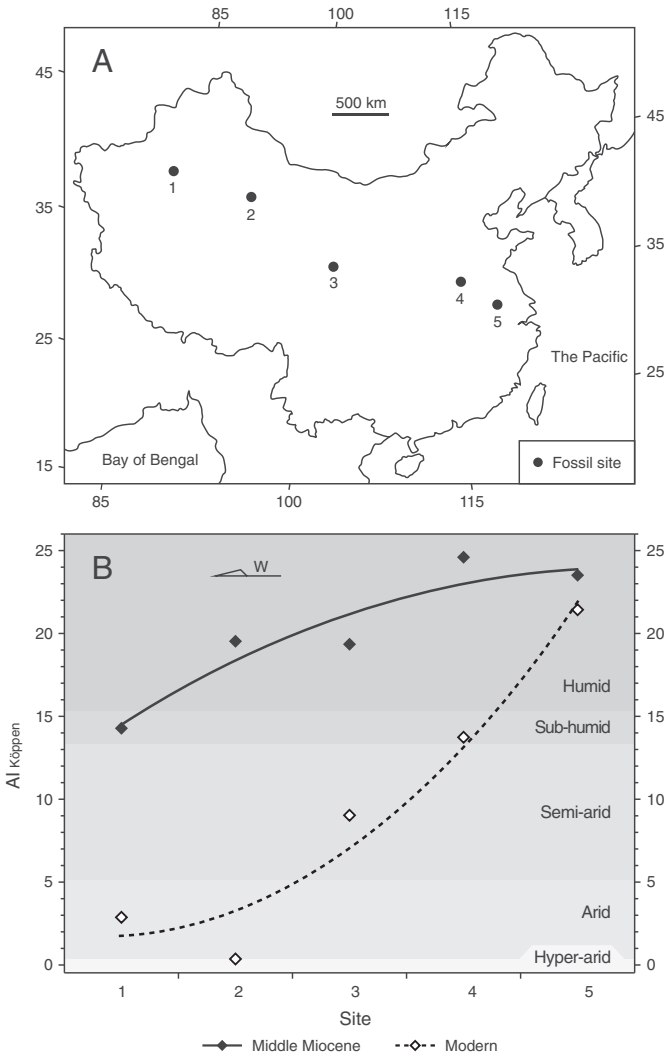

Fig. 4. Westward aridification of China between the Miocene and modern day. A, Location of 5 Chinese middle Miocene sites in the case study as listed in Table 5; B, asymmetric process of aridification from the middle Miocene to the present. Black and gray solid diamonds show the Miocene and corresponding modern localities, respectively, while the black and gray solid lines indicate the overall trend of aridity distribution of particular period.

data ignore the effectiveness of temperature (Thornthwaite, 1948; Walton, 1969; Botzan et al., 1998; Warren, 2006). And more importantly, $AI_{Köppen}$ provides a full categorization that is applicable to both paleo- and modern climate. By using this index, the climate in a particular geological period can be clearly and quantitatively defined.

6. Conclusions

The validation of 5 widely used PT-based aridity indices demonstrates that $AI_{Köppen}$ is the most reliable index for evaluating terrestrial hydrological conditions of a given area. This work represents the first attempt to find a simple quantitative proxy for estimating relative arid condition in the geologic past. The application of $AI_{Köppen}$ in paleoclimate studies requires only two climatic parameters (MAT and MAP), both of which might be readily estimated from geological data or the fossil record, although with some uncertainty. Another key advantage of this index is that it allows estimation of humid-arid dynamics by the same criterion as the modern climate, so that the hydrological process can be directly compared throughout the geological time. The case study of $AI_{Köppen}$ reveals a westward drying of China during the middle Miocene, consistent with the general trend indicated by the lithological evidence. However, it should also be noted that western China was under a sub-humid to humid climate in the middle Miocene, as opposed to an arid cliamte, as previously thought.

Supplementary data to this article can be found online at http://dx.doi.org/10.1016/j.palaeo.2013.05.008.

Acknowledgments

We are grateful to Dr. P. Kershaw (Monash University), Dr. Jean-Pierre Suc (Université Claude Bernard-Lyon 1), and an anonymous reviewer for their constructive comments, and to Mr. Edward Liu for his proof-reading. Funding for this research was provided by the National Basic Research Program of China 2012CB822003 and 2012CB821901, and NSFC 41002004 and 41172008 to C.Q., NSFC and US NSF EAR-0746105 to Y.S.L., and DFG and the BiK F (Loewe Initiative of the Federal State of Hessen) to T.U. This is a contribution to the program "Neogene Climate Evolution in Eurasia—NECLIME."

References

Abels, H.A., Dupont-Nivet, G., Xiao, G., Bosboom, R., Krijgsman, W., 2011. Step-wise change of Asian interior climate preceding the Eocene–Oligocene Transition (EOT). Palaeogeography, Palaeoclimatology, Palaeoecology 299, 399–412.
Akkiraz, M.S., Akgün, F., Utescher, T., Bruch, A.A., Mosbrugger, V., 2011. Precipitation gradients during the Miocene in western and central Turkey as quantified from pollen data. Palaeogeography, Palaeoclimatology, Palaeoecology 304, 276–290.
Arora, V.K., 2002. The use of the aridity index to assess climate change effect on annual runoff. Journal of Hydrology 265, 164–177.
Baltas, E., 2007. Spatial distribution of climatic indices in northern Greece. Meteorological Applications 14, 69–78.
Barbour, M.G., Billings, W.D., 2000. North American Terrestrial Vegetation. Cambridge University Press, Cambridge.
Beran, M.A., Rodier, J.A., 1985. Hydrological aspects of drought, studies and reports in hydrology. UNESCO-WMO, 39. Presses Universitaires de France, Paris 149.
Botzan, M.G., 1974. Consideratii asupra indicilor climatici pentru proiectarea irigatiilor. Hidrotehnica 19, 41–48.
Botzan, T.M., Marino, M.A., Necula, A.I., 1998. Modified de Martonne aridity index: application to the Napa Basin, California. Physical Geography 19, 55–70.
Brachert, T., Brügmann, G., Mertz, D., Kullmer, O., Schrenk, F., Jacob, D., Ssemmanda, I., Taubald, H., 2010. Stable isotope variation in tooth enamel from Neogene hippopotamids: monitor of meso and global climate and rift dynamics on the Albertine Rift, Uganda. International Journal of Earth Sciences 99, 1663–1675.
Bugmann, H.K.M., Solomon, A.M., 2000. Explaining forest composition and biomass across multiple biogeographical regions. Ecological Applications 10, 95–114.
Chaves, M.M., Maroco, J.P., Pereira, J.S., 2003. Understanding plant responses to drought—from genes to the whole plant. Functional Plant Biology 30, 239–264.
Crago, R., Hervol, N., Crowley, R., 2005. A complementary evaporation approach to the scalar roughness length. Water Resources Research 41, W06017.
de Martonne, E., 1926. Aréisme et indice d'aridité. Comptes Rendus de l'Académie des Sciences 182, 1395–1398.
de Martonne, E., 1942. Nouvelle carte mondiale de l'indice d'aridité. Annales de Géographie 51, 242–250.
Emberger, L., 1930. La végétation de la région méditerranéenne: essai d'une classification des groupements végétaux. Revue Générale de Botanique 42 (641–662), 705–721.
Fang, J.Y., Yoda, K., 1989. Climate and vegetation in China II. Distribution of main vegetation types and thermal climate. Ecological Research 4, 71–83.
Fine, P.V.A., Ree, R.H., Burnham, R.J., 2008. The disparity in tree species richness among tropical, temperate, and boreal biomes: the geographic area and age hypothesis. In: Carson, W.P., Schnitzer, S.A. (Eds.), Tropical Forest Community Ecology. Wiley, Oxford, pp. 31–62.
Fortelius, M., Zhang, Z., 2006. An oasis in the desert? History of endemism and climate in the late Neogene of North China. Palaeontographica Abteilung A 227, 131–141.
Gasse, F., 2000. Hydrological changes in the African tropics since the Last Glacial Maximum. Quaternary Science Reviews 19, 189–211.
Greenwood, D.R., Basinger, J.F., Smith, R.Y., 2010. How wet was the Arctic Eocene rain forest? Estimates of precipitation from Paleogene Arctic macrofloras. Geology 38, 15–18.
Guo, Z.T., Sun, B., Zhang, Z.S., Peng, S.Z., Xiao, G.Q., Ge, J.Y., Hao, Q.Z., Qiao, Y.S., Liang, M.Y., Liu, J.F., Yin, Q.Z., Wei, J.J., 2008. A major reorganization of Asian climate by the early Miocene. Climate of the Past 4, 153–174.
Hoorn, C., Straathof, J., Abels, H.A., Xu, Y., Utescher, T., Dupont-Nivet, G., 2012. A late Eocene palynological record of climate change and Tibetan Plateau uplift (Xining Basin, China). Palaeogeography, Palaeoclimatology, Palaeoecology 344–345, 16–38.
Jeffrey, S.J., Carter, J.O., Moodie, K.B., Beswick, A.R., 2001. Using spatial interpolation to construct a comprehensive archive of Australian climate data. Environmental Modelling & Software 16, 309–330.
Köppen, W., 1900. Versuch einer Klassifikation der Klimate, vorzugsweise nach ihren Beziehungen zur Pflanzenwelt. Geographische Zeitschrift 6 (593–611), 657–679.
Köppen, W., 1923. Die Klimate der Erde. Walter de Gruyter & Co., Berlin und Leipzig.
Köppen, W., 1931. Grundriss der Klimakunde. Walter de Gruyter & Co., Berlin und Leipzig.

Kottek, M., Grieser, J., Beck, C., Rudolf, B., Rubel, F., 2006. World Map of the Koppen–Geiger climate classification updated. Meteorologische Zeitschrift 15, 259–263.
Lang, R., 1915. Versuch einer exakten Klassifikation der Böden in klimatischer und geologischer Hinsicht. Internationale Mitteilungen fuer Bodenkunde 5, 312–346.
Lang, R., 1920. Verwitterung und Bodenbildung als Einführung in die Bodenkunde. Schweizerbart Science Publishers, Stuttgart.
Levin, N.E., Cerling, T.E., Passey, B.H., Harris, J.M., Ehleringer, J.R., 2006. A stable isotope aridity index for terrestrial environments. Proceedings of the National Academy of Sciences 103, 11201–11205.
Light, H.M., Darst, M.R., Lewis, L.J., 2002. Hydrology, vegetation, and soils of riverine and tidal floodplain forests of the lower Suwannee River, Florida, and potential impacts of flow reductions. U.S. Geological Survey Professional Paper, 1656A. U.S. Geological Survey, Denver.
Linsser, C., 1869. Untersuchungen über die periodischen Lebenserscheinungen der Pflanzen. II. Resultate aus einer eingehenden Bearbeitung des europäischen Materials für die Hclzpflanzen in bezug auf Wärme und Regenmenge. Mémoires de l'Académie Impériale des Sciences de St. Petersbourg 13, 1–87.
Liu, L., Eronen, J.T., Fortelius, M., 2009. Significant mid-latitude aridity in the middle Miocene of East Asia. Palaeogeography, Palaeoclimatology, Palaeoecology 279, 201–206.
Liu, Y.S., Utescher, T., Zhou, Z., Sun, B., 2011. The evolution of Miocene climates in North China: preliminary results of quantitative reconstructions from plant fossil records. Palaeogeography, Palaeoclimatology, Palaeoecology 304, 308–317.
Moreno, J.M., Pineda, F.D., Rivas-Martinez, S., 1990. Climate and vegetation at the Eurosiberian-Mediterranean boundary in the Iberian Peninsula. Journal of Vegetation Science 1, 233–244.
Mosbrugger, V., Utescher, T., 1997. The coexistence approach—a method for quantitative reconstructions of Tertiary terrestrial palaeoclimate data using plant fossils. Palaeogeography, Palaeoclimatology, Palaeoecology 134, 61–86.
Müller, M.J., 1996. Handbuch Ausgewählter Klimastationen der Erde. Forschungsstelle Bodenerosion der Universität Trier, Mertesdorf.
Murphy, B.F., Timbal, B., 2008. A review of recent climate variability and climate change in southeastern Australia. International Journal of Climatology 28, 859–879.
Parrish, J.T., 1998. Interpreting pre-Quaternary climate from the geologic record. Columbia University Press, New York.
Peel, M.C., Finlayson, B.L., McMahon, T.A., 2007. Updated world map of the Köppen-Geiger climate classification. Hydrology and Earth System Sciences 11, 1633–1644.
Penck, A., 1910. Versuch einer Klimaklassifikation auf physiogeographischer Grundlage. Sitzungsberichte der Preussischen Akademie der Wissenschaften 12, 236–246.
Quan, C., Liu, Y.-S.C., Utescher, T., 2012. Paleogene temperature gradient, seasonal variation and climate evolution of northeast China. Palaeogeography, Palaeoclimatology, Palaeoecology 313–314, 150–161.
Retuerto, R., Carballeira, A., 1992. Use of direct gradient analysis to study the climate-vegetation relationships in Galicia, Spain. Plant Ecology 101, 183–194.
Roberts, B.R., 1993. Water management in desert environments: a comparative analysis. Springer, Berlin.
Rubel, F., Kottek, M., 2010. Observed and projected climate shifts 1901–2100 depicted by world maps of the Köppen-Geiger climate classification. Meteorologische Zeitschrift 19, 135–141.
Schneider, T., O'Gorman, P.A., Levine, X.J., 2010. Water vapor and the dynamics of climate changes. Reviews of Geophysics 48, RG3001.
Shahid, S., 2010. Spetio-temporal variation of aridity and dry period in term of irrigation demand in Banglades. American-Eurasian Journal of Agricultural & Environmental Sciences 7, 386–396.
Spicer, R.A., Valdes, P.J., Spicer, T.E.V., Craggs, H.J., Srivastava, G., Mehrotra, R.C., Yang, J., 2009. New developments in CLAMP: calibration using global gridded meteorological data. Palaeogeography, Palaeoclimatology, Palaeoecology 283, 91–98.
Stadler, S.J., 2005. Aridity indexes. In: Oliver, J.E. (Ed.), The Encyclopedia of World Climatology. Springer, Dordrecht, pp. 89–94.
Su, T., Xing, Y.W., Liu, Y.S., Jacques, F.M.B., Chen, W.Y., Huang, Y.J., Zhou, Z.K., 2010. Leaf margin analysis: a new equation from humid to mesic forests in china. Palaios 25, 234–238.
Sun, X., Wang, P., 2005. How old is the Asian monsoon system?—Palaeobotanical records from China. Palaeogeography, Palaeoclimatology, Palaeoecology 222, 181–222.
Thornthwaite, C.W., 1948. An approach toward a rational classification of climate. Geographical Review 38, 55–94.
Tsakiris, G., Vangelis, H., 2004. Towards a drought watch system based on spatial SPI. Water Resources Management 18, 1–12.
Tuhkanen, S., 1980. Climatic parameters and indices in plant geography. Acta Phyogeographica Suecica 67, 1–105.
Utescher, T., Bruch, A.A., Micheels, A., Mosbrugger, V., Popova, S., 2011. Cenozoic climate gradients in Eurasia—a palaeo-perspective on future climate change? Palaeogeography, Palaeoclimatology, Palaeoecology 304, 351–358.
Wallén, C.C., 1967. Aridity definitions and their applicability. Geografiska Annaler Series A Physical Geography 49, 367–384.
Walter, H., 1973. Vegetation of the Earth in Relation to Climate and the Eco-physiological Conditions. Springer, New York.
Walton, K., 1969. The Arid Zones. Aldine Publishing Company, Chicago.
Warren, J.K., 2006. Evaporites sediments, resources and hydrocarbons. Springer, Berlin.
Wilf, P., 1997. When are leave good thermometers? A new case for leaf margin analysis. Paleobiology 23, 373–390.
Wilhite, D.A., Glantz, M.H., 1985. Understanding the drought phenomenon: the role of definitions. Water International 10, 111–120.
Wing, S.L., Greenwood, D.R., 1993. Fossils and fossil climates: the case for equable continental interiors in the Eocene. Philosophical Transactions of the Royal Society of London, B 341, 243–252.
Wolfe, J.A., 1993. A method of obtaining climatic parameters from leaf assemblages. U.S. Geological Survey Bulletin 2041, 1–71.
Woodward, F.I., Lomas, M.R., Kelly, C.K., 2004. Global climate and the distribution of plant biomes. Philosophical Transactions of the Royal Society of London. Series B, Biological Sciences 359, 1465–1476.
Yan, Z., Petit-Maire, N., 1994. The last 140 ka in the Afro-Asian arid/semi-arid transitional zone. Palaeogeography, Palaeoclimatology, Palaeoecology 110, 217–233.
Yechieli, Y., Wood, W.W., 2002. Hydrogeologic processes in saline systems: playas, sabkhas, and saline lakes. Earth-Science Reviews 58, 343–365.
Zhang, C., Wang, Y., Li, Q., Wang, X., Deng, T., Tseng, Z.J., Takeuchi, G.T., Xie, G., Xu, Y., 2012. Diets and environments of late Cenozoic mammals in the Qaidam Basin, Tibetan Plateau: evidence from stable isotopes. Earth and Planetary Science Letters 333–334, 70–82.
Ziegler, A.M., Eshel, G., Rees, P.M., Rothfus, T.A., Rowley, D.B., Sunderlin, D., 2003. Tracing the tropics across land and sea: Permian to present. Lethaia 36, 227–254.